Broadband Electron Spin Resonance Using Superconducting Coplanar Waveguide

C. Clauss, D. Bothner, D. Koelle, R. Kleiner, L. Bogani, M. Scheer, and M. Dressel
Physikalisches Institut, Universit at Stuttgart, Germany

Jie Zhang

11/14/2013

Outline

- ESR detection technique
- Experimental setup
- Field sweeping
- Frequency sweeping
- Design

Electron spin resonance

- Electron spin resonance (ESR) or Electron paramagnetic resonance (EPR) spectroscopy is a technique for studying materials with unpaired electrons;
- Zeeman effect: $E = m_s g \mu_B B_0$

  where g is the electron's Landé g-factor.

  For the free electron, $g = 2.0023$, μ_B is the Bohr magneton
- Resonance absorption: $\Delta E = g \mu_B B_0$

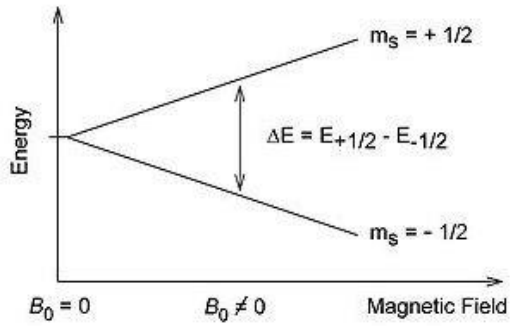

- DPPH signal: $g = \frac{\hbar \omega}{\mu_B B} = 1.9934$

  Line width: 150 Gauss

Fitting with a Lorentzian: $\boxed{L(B) = \frac{A}{1+[(\frac{\mu g \tau}{h})(B-B_r)]^2}} \Rightarrow \tau = 7.78ns$

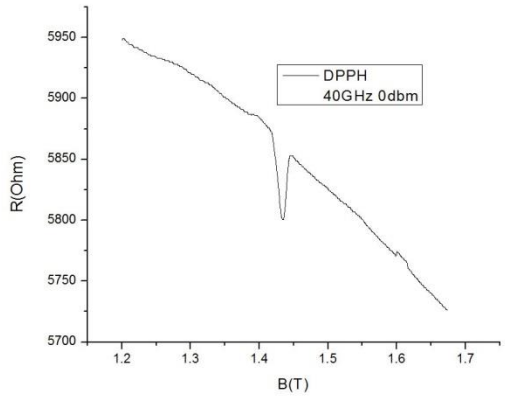

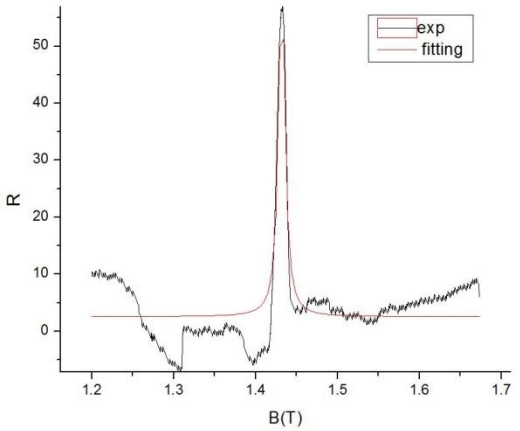

ESR detection techniques

- Conventional method (commercialized): transmission spectroscopy----measuring the absorption or transmission coefficient ;
- Magnetic torque detection: measuring the change that a magnetic resonance transition induces in the magnetization of the system;

$$\tau = M \times B$$

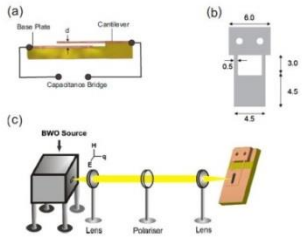

FIG. 1. (Color online) A drawing of (a) the torque meter with the cantilever placed at a distance d from the base plate, (b) the cantilever (all dimensions are in millimeter), and (c) the quasioptical setup which illustrates how the beam is focused onto the single crystal located on the cantilever.

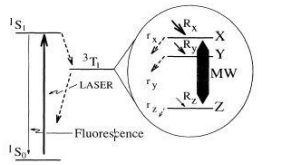

FIG. 1. Energy level scheme showing the singlet ground state $^1S_0$, the first excited state $^1S_1$, and the lowest excited triplet state $^3T_1$. The energy separation of $^1S_1$ and $^1S_0$ is $\sim$16883 cm^{-1}; that of $^3T_1$ and $^1S_0$ is estimated to be $\sim$10000 cm^{-1} [17]. Populating and depopulating rates of the triplet sublevels are denoted by $R_{X,Y,Z}$ with $R_X \sim 66$ kHz, $R_Y \sim 29$ kHz, $R_Z \sim 0.28$ kHz, and $r_{X,Y,Z}$ with lifetimes $r_{X,Y}^{-1} \sim 47$ μs and $r_Z^{-1} \sim 830$ μs, respectively [10].

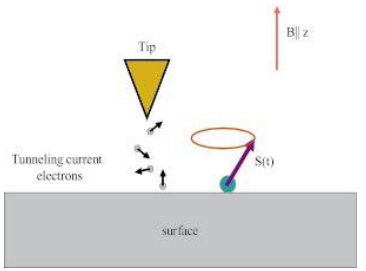

- Optically detected ESR;
- STM-ESR;
- Resistively detection: measuring the longitudinal resistance of 2DEG(Landau Level, Zeeman Splitting, filling factor);
- Thermal detection: measuring the temperature change induced by the non-radiative relaxation of the photon absorption;

Challenges to be improved regarding ESR

- Sensitivity---- resonant cavities
- Bandwidth of fields
- Bandwidth of frequency----small size cavity offers quasi-optical region (50-100GHz) resonance, coupled antenna approach or tunable cavities resolve low frequency range
- Material dependence

Radio frequency field generated by microfabricated superconducting coplanar waveguide

Purpose:

- In order to probe both the frequency and field dependence of ESR line in a wide range (0.5-40GHz)
- Precisely determined the zero field splitting (D-values in the spin Hamiltonian)

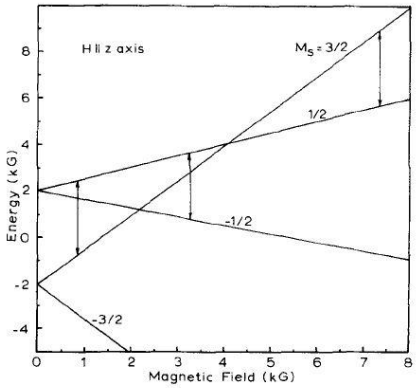

FIG. 3. Cr^{3+} fine-structure energy level diagram of the magnetic complex (1) in GAlSeH when the magnetic field is along the z axis.

- Resolve high order anisotropy terms of multilevel spin systems (play an important role in rare earth coordination compounds)

Experimental setup

- Signal carried by the center conductor line is flanked by two ground planes which act as the outer shielding

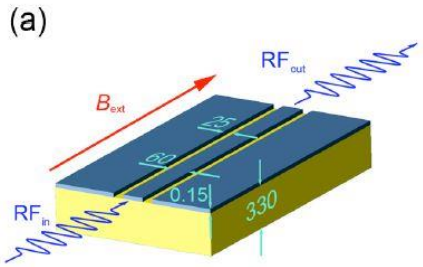

TABLE I. Crystal orientations of sample disks in this study. Directions of shock propagation are perpendicular to flat surfaces of disks, which are labeled with four hexagonal indices; Θ is angle between normal to each disk and c axis. c_l is longitudinal sound speed.

Orientation	Four indices	Θ °	c_l km/s
c-cut	(0001)	0	11.19
d-cut	$(10\bar{1}4)$	38	10.95
r-cut	$(1\bar{1}02)$	57	10.60
n-cut	$(11\bar{2}3)$	61	10.85
s-cut	$(10\bar{1}1)$	72	11.20
g-cut	$(11\bar{2}1)$	79	11.11
m-cut	$(10\bar{1}0)$	90	11.21

- Device fabricated by sputtering a 150nm thick niobium film on the top of a 330μm thick r-cut sapphire substrate and structuring the film with UV lithography
- Critical temperature of Niobium is $T_C = 9K$
- The chip (7x4mm^2)is mounted into a gold plated brass box and contacted with silver paste between the box and ground planes.
- Sample preparation:

1. Dissolve a small amount of crystallites in isopropyl and dropwise transfer to the waveguide and the radials were permanently attached to the waveguide after evaporation of the solvent (NITPhOMe)
2. A polished brick-shaped crystal was put directly onto the chip and fixed with vacuum grease (Ruby)

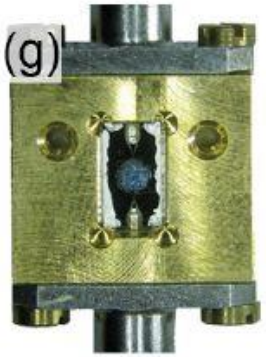

Experimental setup (continued)

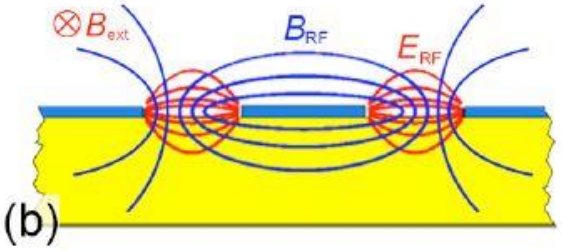

- All data were acquired at 1.6 K cooled by a magnet cryostat where the external magnetic field is oriented parallel to the film
- The magnetic component of the microwave signal is perpendicular to the static external field thus satisfying the condition to flip the spin between Zeeman-split levels
- The waveguide meanders over the chip and only parts of it are oriented in the correct way (much stronger signal for design in (f))
- A CW microwave signal (-20dbm=0.01mW) is fed via coaxial cables to the sample and the transmitted power is recorded with a power meter (NITPhOMe (c)) or with a vector network analyzer (Ruby (d))

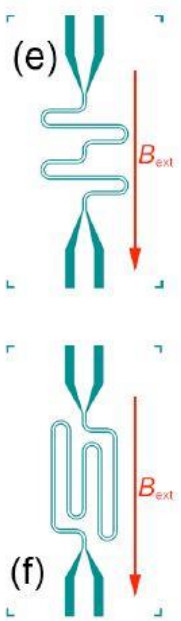

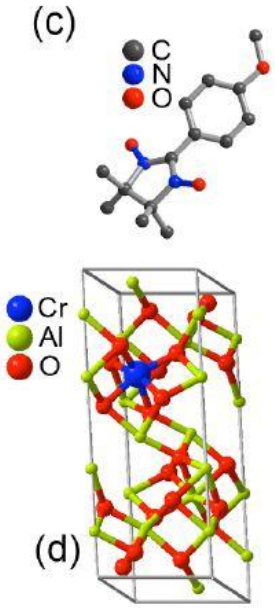

Transmission spectrum (frequency swept)

- The transmission decreases with the increasing frequency steadily up to 33GHz due to the frequency-dependent attenuation of the coaxial cables and the coplanar line
- For frequency above 25GHz, the measured transmitted power is close to the detection limit of the power meter and the spectra get very noisy
- The signal intensity increases with increasing external field due to the increasing thermal population difference of the Zeeman split energy levels.
- A g-factor of $g = 2.019 \pm 0.001$ can be extracted from the slop of the absorption peak vs. external magnetic field
- All possible transitions between the four states of the zero-field-split quartet can be seen from the normalized frequency-swept ESR spectra for Ruby
- This method is suitable to determine the weight of higher order anisotropy terms for more complex materials

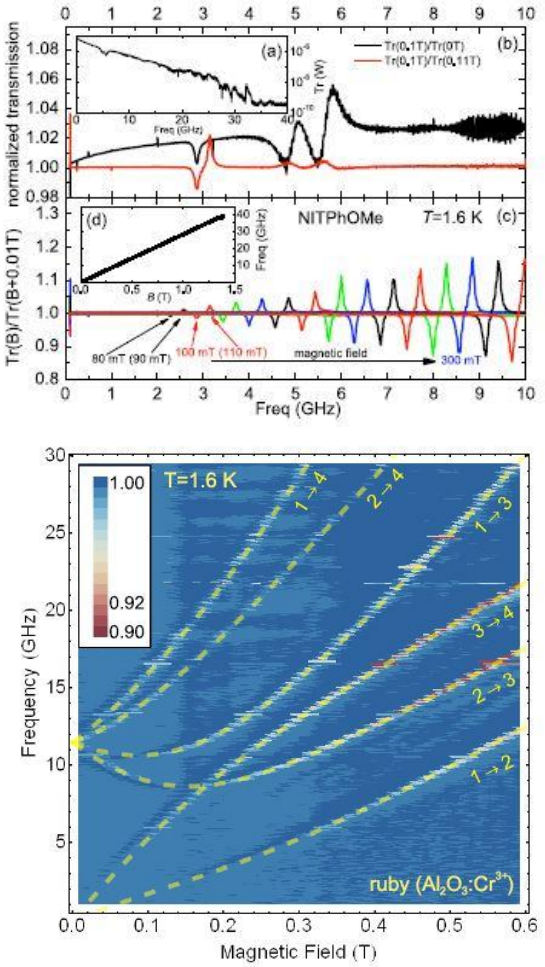

FIG. 3: (color online) Normalized frequency-swept ESR spectra for ruby. Lighter and red areas show the ESR absorption positions and dashed lines show a fit to the transitions between the eigenfunctions of the Cr^{3+} spin Hamiltonian. The different spin states are labeled as 1: $m_s = -\frac{3}{2}$, 2: $m_s = -\frac{1}{2}$, 3: $m_s = +\frac{1}{2}$ and 4: $m_s = +\frac{3}{2}$

Transmission spectrum (field swept)

- The off-resonance transmission decreases with increasing field/frequency due to the frequency dependent attenuation
- ESR can be detected with frequency as high as 40GHz

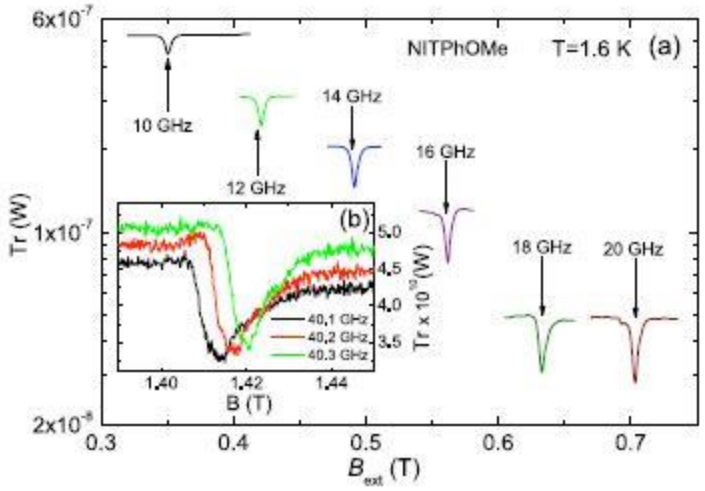

FIG. 4: (color online) (a) Field-swept spectra for various frequencies. The absolute value of the transmitted power off-resonance is predominantly determined by the frequency-dependent damping of the coaxial lines. Inset (b): Field swept spectra around 40 GHz.

Temperature dependence

- The high frequency losses of the waveguide are minimized when working below T_C, it is also possible to resolve ESR signal at temperature above T_C (for $B_{ext} = 1\,T, T_C = 5K$);
- An increasing of the peak amplitude can be observed due to the increasing of imbalance of thermal occupation;
- Two effects can be seen when reaching critical temperature:

(1) While crossing the transition temperature, the baseline deviates from unity due to the different transport properties of the metallic film for the spectra recorded at $B_{ext} = 1\,T$ compared to the reference spectra at $B_{ext} = 1.05T$;

(2)Below T_C, the peak frequency shifts to slightly higher frequencies and the absorption dip gets broadened.

Attributed to the modification of the local magnetic field by shielding current in the superconductor:
The magnetic field is enhanced at the surface of the Nb planes and in the gaps between the center and the ground planes compared to the normal conducting states which shifts the Zeeman splitting of spins sitting directly at the surface to higher values. With increasing distance from the Nb surface the field approach B_{ext} and due to this field inhomogeneity we not only get a shift but also a broadening of the ESR absorption dip.

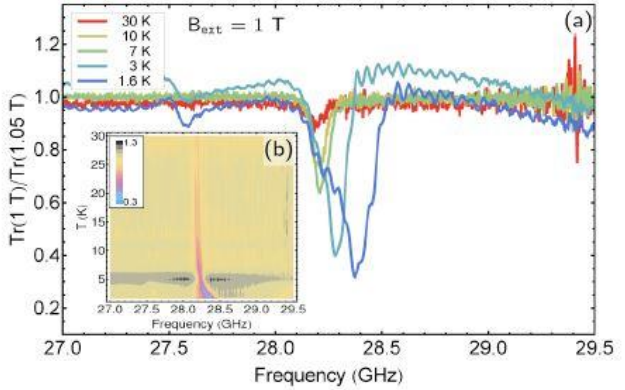

FIG. 5: (color online) (a) frequency-swept spectra for several selected temperatures. The absorption is already visible for temperatures above T_c. Upon cooling through the superconducting transition, the absorption peak frequency shifts to higher frequencies. (b) All measured spectra shown in a contour map. The transition into the superconducting state around 5 K as well as the shift of the ESR absorption for temperatures below T_c is clearly visible.

Design

- Operates at 300mK
- Brass box
- Meander line

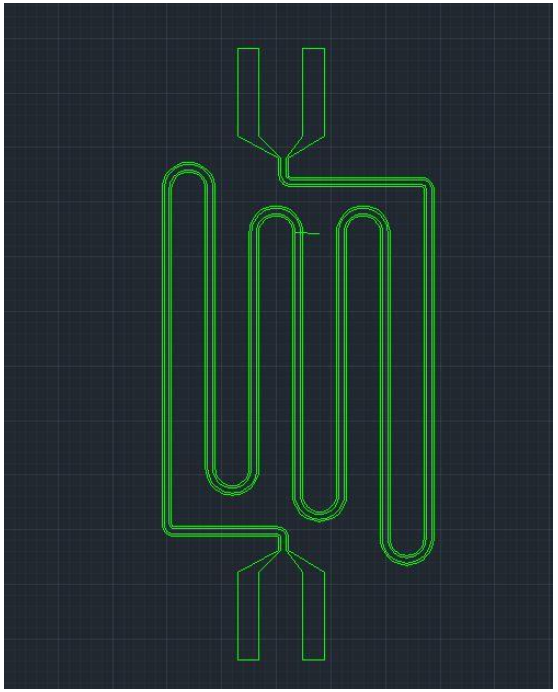

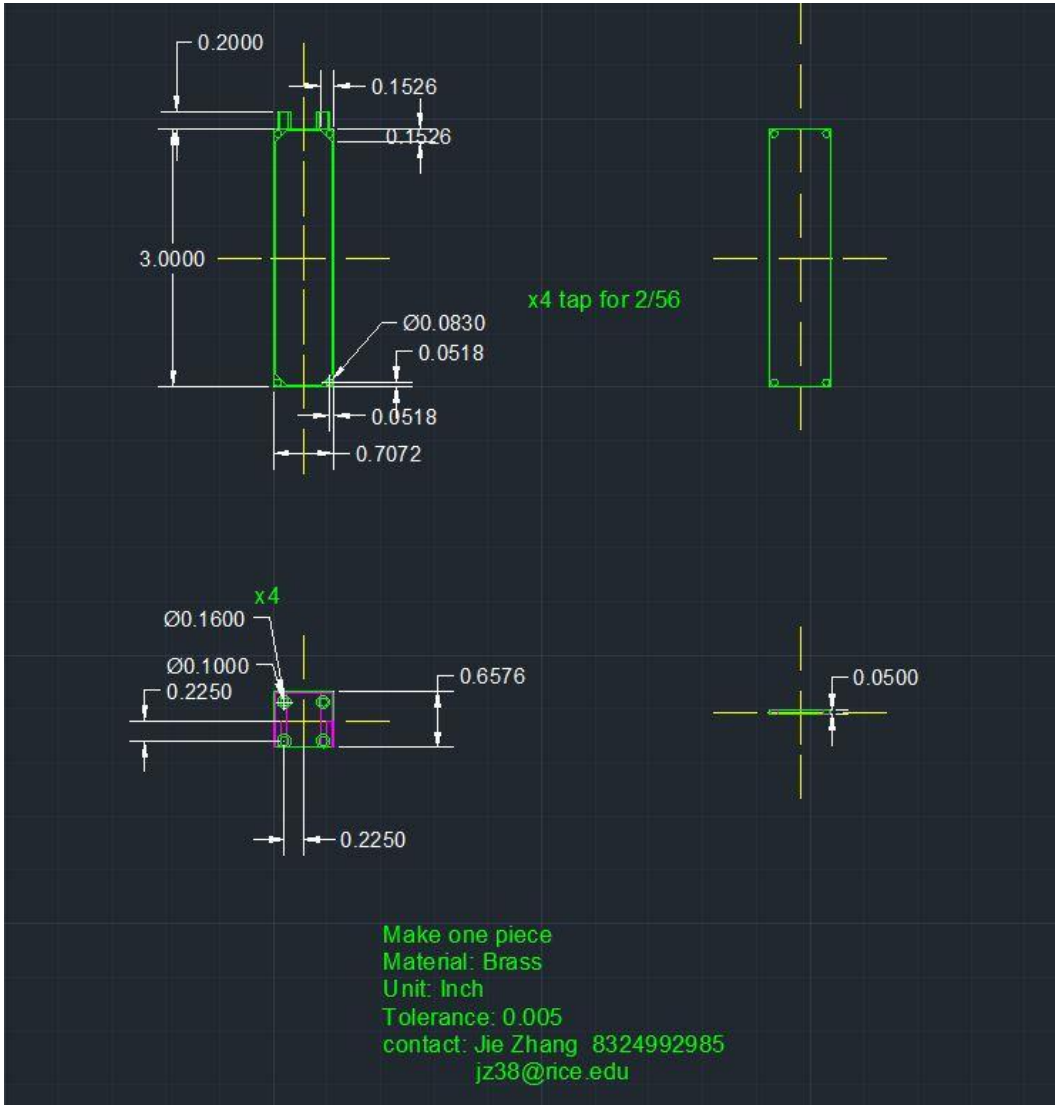

Reference

[1] Broadband electron spin resonance from 500 MHz to 40 GHz using superconducting coplanar waveguides Applied Physics Letters 102, 162601 (2013)

[2] High-Cooperativity Coupling of Electron-Spin Ensembles to Superconducting Cavities PRL 105, 140501 (2010)

[3] Torque detected broad band electron spin resonance REVIEW OF SCIENTIFIC INSTRUMENTS 81, 095105 2010

[4] P. N. Murgatroyd and M. Belloufi, *A sensitive differential thermometer.* Meas. Sci. Technol. 1 (1990)

[5] ESR-STM of a single precessing spin: Detection of exchange-based spin noise PRB 66, 195416 2002

[6] Optically Detected Spin Coherence of Single Molecules PhysRevLett.71.3565

[7] Electron spin resonance measurements of the spin Hamiltonian zerofield splitting parameter D as a function of temperature for trigonally distorted Cr3+6H2O magnetic complexes in families of hydrated crystals. The Journal of Chemical Physics **63**, 4450 (1975); doi: 10.1063/1.431165

[8] Response of seven crystallographic orientations of sapphire crystals to shock stresses of 16–86 GPaJ. Appl. Phys. 106, 043524 2009